ARCHIVES of FOUNDRY ENGINEERING

Published quarterly as the organ of the Foundry Commission of the Polish Academy of Sciences

ISSN (1897-3310)
Volume 15
Issue 3/2015

71 – 76

15/3

X-ray Diffraction Study of Directional Solidification Ledeburite

M. Trepczyńska-Łent *, T. Szykowny
Department of Materials Science and Engineering, Mechanical Engineering Faculty,
UTP University of Science and Technology, al. Kaliskiego 7, 85-796 Bydgoszcz, Poland
*Corresponding author. E-mail address: malgorzata.trepczynska-lent@utp.edu.pl

Received 04.05.2015; accepted in revised form 29.05.2015

Abstract

Directionally solidified sample of Fe-Fe_3C eutectic alloy were produced under an argon atmosphere in a vacuum Bridgman-type furnace to study the eutectic growth with v = 167 μm/s pulling rate and constant temperature gradient G = 33.5 K/mm. Since how the growth texture of eutectic cementite is related to its growth morphology remains unclear, the current study aims to examine this relationship. The technique such as X-ray diffraction, have been used for the crystallographic analysis of carbide particles in white cast irons.

Keywords: X-ray diffraction, Ledeburite eutectic, Directional solidification

1. Introduction

Eutectic alloys can form a variety of different two-phase microstructures during the liquid/solid phase transformation. Because of their superior mechanical properties associated with a fine-scale composite microstructure, eutectic alloys have attracted much attention in the realm of materials science. In addition, the use of eutectic materials as in situ composites is of great interest to metallurgists.

Ledeburite consists of eutectic cells in which many austenite rods, along [001], are embedded into cementite platters (or blocks) based on (001) plane. The eutectic cells show a lamellar or plate shape; their length and width are far greater than their thickness. Therefore, under microscope, only the transverse sections of the austenite rods are observed. After etching, they show as dark round spots on a white cementite [1].

Orthorhombic cementite, Fe_3C, has many more Bragg peaks of much smaller intensity than cubic ferrite and is, therefore, difficult to study by X-ray diffraction. Satisfactory were obtained results using a specimen containing 4.37 wt.% carbon, which is close to the eutectic composition (4.3 wt.%). The total cementite content amounts to 65.5 vol.%, 9% of which are needles of primary cementite with random crystallographic orientation. A fraction of 81% of the cementite consists of lamellar eutectic and secondary cementite and is preferentially oriented with its *b*-axis parallel to the direction of heat flow during eutectic solidification [2]. This direction is perpendicular to the surface, which we investigated by X-ray diffraction. The remaining cementite, and all of the ferrite, is contained in the heterogeneous pearlite phase. The pearlite particles consist of alternating ferrite and cementite lamellae with a periodicity on the submicrometer scale. The lamellae have more or less well defined orientation relationships [3]. For the theoretical considerations were assumed that they are oriented perpendicular to the [110] and [001] directions of ferrite and cementite, respectively [4].

At room temperature, the lattice parameters of cementite amount to a = 0.45165 nm; b = 0.50837 nm and c = 0.67475 nm [5]. Cementite is ferromagnetic with the direction of magnetization parallel to the *c*-axis [6].

White cast iron consists of the phases ferrite and cementite. On cooling, strong thermoelastic stresses $\Delta\sigma_{ij}$ occur which-because of equilibrium conditions-have different signs in the two phases. According to the $sin^2\psi$ - law of conventional X-ray stress

analysis (ψ is the angle between the reflecting lattice plane and the irradiated surface of the specimen), the corresponding thermo-elastic strains Δd of the lattice plane spacings, if plotted versus $sin^2\psi$, should yield straight lines with slopes proportional to $\Delta\sigma_{ij}$ components. The slopes observed for the two phases should, therefore, have different signs. Experimentally, the opposite was observed. It is shown that this unexpected behaviour is related to the anisotropic microscopic thermal expansion coefficients of the cementite combined with anisotropic macroscopic thermal expansion coefficients of the specimen. The latter is a result of the texture of the cementite phase. This changes more or less the conventionally expected $\Delta d(sin^2\psi)$ curves of the two phases [6].

Researched rapidly solidified binary Fe–C alloys containing 3.8 wt% and 4.3 wt% C. Their microstructure reveals that, as an effect of undercooling, the conventional eutectics have been suppressed and there is occurrence of the ferrite–cementite eutectic. Both phases are metastable: ferrite is supersaturated in C and cementite has a C deficiency. This is demonstrated by means of determination of phase fractions in metallographic sections and of lattice parameters via Rietveld refinement of X-ray diffraction patterns. A major consequence of non-stoichiometricity of cementite is the reduced value of the Curie temperature (up to 17°C) with respect to that of the equilibrium compound. The maximum C deficiency in Fe_3C_{1-x} is estimated as x = 0.02. The free energy of defective cementite has been computed by means of the two sublattice model and compared with that of ferrite and austenite obtained from an assessed phase diagram. It is shown that the non-stoichiometric phase is close in energy to the equilibrium one for a composition range of several atomic per cent. It is suggested that this helps in explaining the mechanism of cementite dissolution by heavy deformation of ferrous alloys, and the ease of cementite nucleation in castings [7].

In the work [8] was a greater insight into the extremely anisotropic elastic properties of Fe_3C presented. The observed anisotropy was confirmed experimentally by X-ray diffraction stress measurements on macrostressed, massive, polycrystalline Fe_3C layers grown on a-Fe substrates.

2. Experimental procedure

The Fe – 4.3 wt.% C eutectic sample were prepared from Armco and pure graphite electrodes purity in a graphite crucible under the protection of argon gas in Balzers-type heater. After dross removal and homogenization, the molten alloy was poured into a permanent mold and cast into rod 12 mm in diameter. The specimen were then machined to approximately 5 mm in diameter using a wire cutting process because of the high brittleness of the metals at this composition. After that, the samples were positioned in a alunde tube with an inner diameter of 6 mm at the center of the vacuum Bridgman-type furnace. Under an argon atmosphere, the samples were heated to a temperature of 1450°C. After stabilizing the thermal conditions, the samples were lowered at a given rate from the heating part to the cooling part of the furnace, with Ga-In-Sn liquid metal used as the coolant. The specimen was grown by pulling it downwards at a constant pulling rate $v=167$ μm/s and at a constant temperature gradient $G=33.5$ K/mm by means of motor. This is described in more detail in [9].

The research of directional solidification were performed in the Department of Casting at the AGH University of Science and Technology in Cracow.

2.1. Microstructure research

After being mechanically ground, polished and etched (wit nital) the microstructure of the sample was examined using a light optical microscope. The microstructure of sample were photographed on the longitudinal section.

Figure 1 show the polished and etched sample with marked growth direction and the area of microstructure analysis on the directional solidification sample. The eutectic structure on the Figure 2a) – A, 2b) – B and 2c) – C are represented, respectively.

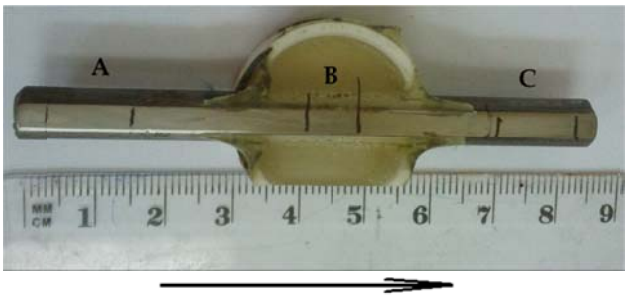

Growth direction

Fig. 1. The image of the research sample and area of microstructure analysis on the sample

Microstructure of ledeburite eutectic from area A, B and C (on the Figure 1) show Figure 2. Only the area B has a directional ledeburite eutectic. The area A of the bottom of the sample and the area C of the top specimen note have directional structure.

2.2. X-ray diffraction of ledeburite

The directional solidification sample has been X-ray investigations. The X-ray investigations of the specimen of ledeburite were performed by means of Co Kα radiation. The inspected surface, which were called the A, B and C area was longitudinal to the direction of growth during solidification. Were observed a texture of the cementite.

Used radiation lamps with cobalt anode and a iron filter. Diffractograms were recorded in the range 2- theta angle of 40° to 80° in steps of 0.02°. The length of the radiation was 0.179021 nm. A diffraction pattern records the X-ray intensity as a function of 2-theta angle.

X-ray diffraction analysis is based on constructive interference of monochromatic X-rays and a crystalline sample. The X-rays are generated by a cathode ray tube, filtered to produce monochromatic radiation, collimated to concentrate, and directed toward the sample. The interaction of the incident rays with the sample produces constructive interference (and a diffracted ray) when conditions satisfy Bragg's law ($n\lambda=2d\ sin\ \theta$). This law

relates the wavelength of electromagnetic radiation to the diffraction angle and the lattice spacing in a crystalline sample [10].

The characteristic X-ray diffraction pattern generated in a typical analysis provides a unique "fingerprint" of the crystals present in the sample. When properly interpreted, by comparison with standard reference patterns and measurements, this fingerprint allows identification of the crystalline form [10].

a)

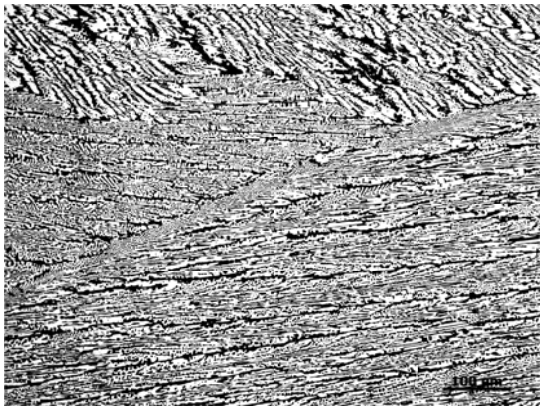

b)

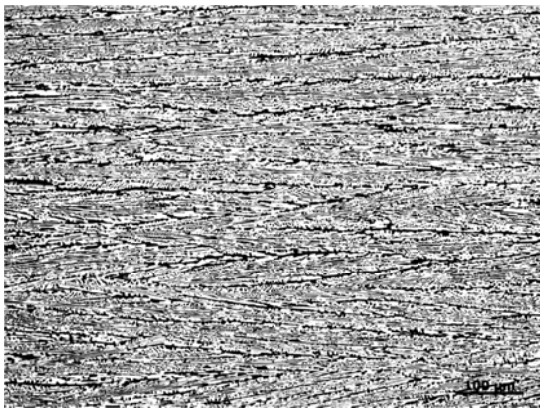

c)

Fig. 2. Microstructure of ledeburite eutectic on the longitudinal section from Figure 1: a) - A, b) - B and c) – C, respectively

3. Experimental results

A diffractograms from an X-ray diffraction are shows on the Figure 3÷7. Figure 4 show diffractometer trace from area A on the specimen (Fig. 1). Figure 4 show X-ray diffraction patterns from area B, when the measurement was made parallel to the axis of the goniometer (B1). Figure 5 - area B, but perpendicular to the axis (B2), and Figure 6 parallel to the axis in place B when the specimen was included in the resin (B3) - as shown in Figure 1.

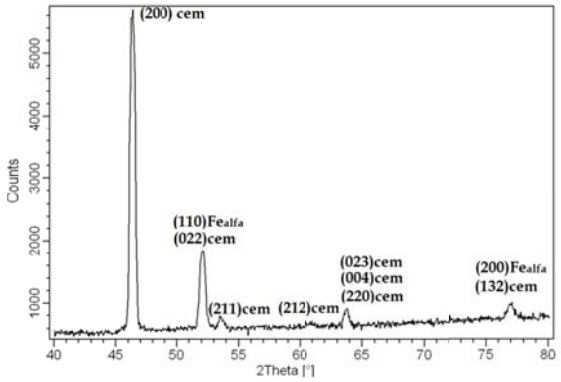

Fig. 3. Diffractometer trace for area A (Fig. 1)

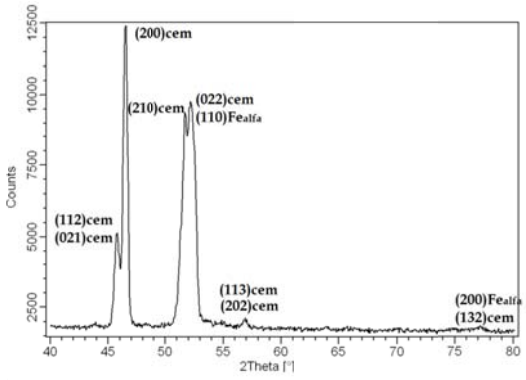

Fig. 4. Diffractometer trace for area B parallel (B1) to the axis of the sample (Fig. 1)

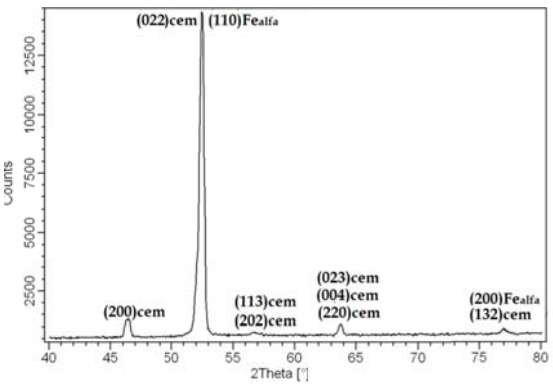

Fig. 5. Diffractometer trace for area B diagonally (B2) to the axis of the sample (Fig. 1)

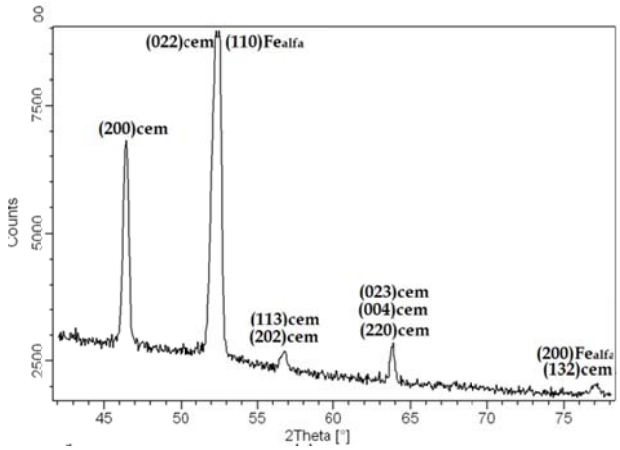

Fig. 6. Diffractometer trace for area B for sample included (B3) in the resin (Fig. 1)

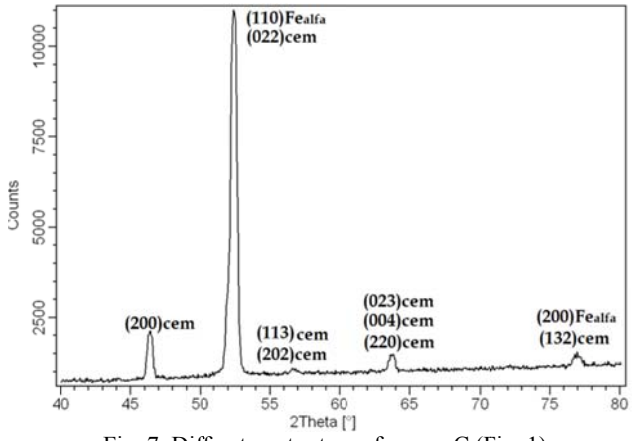

Fig. 7. Diffractometer trace for area C (Fig. 1)

4. Analysis of X-ray diffraction

Results of X-ray diffraction tests are presented in Table 1.

Table1.
Parameters of reflections of the analysed phases

Research of area A (Fig. 3)				Catalog of reflections list [5]					
				Fe_3C			Fe_α		
Peak	2θ	d_{hkl}	I/I_{max}	d_{hkl}	hkl	I/I_{max}	d_{hkl}	hkl	I/I_{max}
1	46.36	0.22725	100.00	*0.225825*	*200*	*24.0*			
2	52.11	0.20360	24.20	*0.203014*	*022*	*48.6*	*0.20268*	*110*	*100*
3	53.56	0.19852	3.03	*0.197354*	*211*	*48.2*	---		
4	60.86	0.17661	1.03	*0.179052*	***212***	*18.4*	---		
5	63.76	0.16936	5.20	*0.168442*	*023*	*13.0*	---		
				0.169922	*220*	*0.2*			
				0.168987	*004*	*4.8*			
6	76.96	0.14375	4.72	*0.143574*	*132*	*0.5*	*0.14332*	*200*	*19*
Research of area B1 (Fig. 4)									
1	45.51	0.23126	31.47	*0.237867*	*021*	*5.9*	---		
	45.76	0.23006	31.47	*0.238655*	*112*	*27.0*			
2	46.51	0.22655	100.00	*0.225825*	*200*	*24.0*	---		
3	51.71	0.20511	71.02	***0.206379***	*210*	*50.0*	---		
4	52.16	0.20347	73.52	*0.203014*	*022*	*48.0*	*0.20268*	*110*	*100*
5	56.91	0.18773	2.35	*0.187664*	*202*	*1.1*	---		
				0.187188	*113*	*30.0*			
6	77.16	0.14344	1.40	*0.143574*	*132*	*0.5*	*0.14332*	*200*	*19*
Research of area B2 (Fig. 5)							Catalog of reflectoins list [5]		
				Fe_3C			Fe_α		
Peak	2θ	d_{hkl}	I/I_{max}	d_{hkl}	hkl	I/I_{max}	d_{hkl}	hkl	I/I_{max}
1	46.46	0.22678	5.49	*0.225825*	*200*	*24.0*	---		
2	52.46	0.20238	100.00	*0.203014*	*022*	*48.6*	*0.20268*	*110*	*100*
3	56.66	0.18849	0.86	*0.187664*	*202*	*1.1*	---		
				0.187188	*113*	*30.0*			
4	63.81	0.16925	3.38	*0.168442*	*023*	*13.0*	---		
				0.168822	*220*	*0.2*			
				0.168687	*004*	*4.8*			
5	77.01	0.14367	1.29	*0.143574*	*132*	*0.5*	*0.14332*	*200*	*19*

Research of area B3 (Fig. 6)				Catalog of reflectoins list [5]					
				Fe_3C			Fe_α		
Peak	2θ	d_{hkl}	I/I_{max}	d_{hkl}	*hkl*	I/I_{max}	d_{hkl}	*hkl*	I/I_{max}
1	46.41	0.22701	62.98	*0.225825*	*200*	*24.0*	---		
2	52.51	0.20220	100.00	*0.203014*	*022*	*48.0*	*0.20268*	*110*	*100*
3	56.81	0.18804	6.19	*0.187664*	*202*	*1.1*	---		
				0.187188	*113*	*30*			
4	63.86	0.16913	12.96	*0.168442*	*023*	*13.0*	---		
				0.168822	*220*	*0.2*			
				0.168987	*004*	*4.8*			
5	76.81	0.14399	2.46	*0.143574*	*132*	*0.5*	*0.14332*	*200*	*19*
6	77.16	0.14344	3.30	*0.143574*	*132*	*0.5*	*0.14332*	*200*	*19*
Research of area C (Fig. 7)				Catalog of reflectoins list [5]					
				Fe_3C			Fe_α		
Peak	2θ	d_{hkl}	I/I_{max}	d_{hkl}	*hkl*	I/I_{max}	d_{hkl}	*hkl*	I/I_{max}
1	46.36	0.22725	12.34	*0.258825*	*200*	*24.0*	---		
2	52.41	0.20256	100.00	*0.203014*	*022*	*48.6*	*0.20268*	*110*	*100*
3	56.66	0.18849	0.98	*0.187664*	*202*	*1.1*	---		
				0.187188	*113*	*30.0*			
4	63.76	0.16936	4.20	*0.168442*	*023*	*13.0*	---		
				0.168822	*220*	*0.2*			
				0.168687	*004*	*4.8*			
5	76.96	0.14375	2.67	*0.143574*	*132*	*0.5*	*0.11332*	*200*	*19*

Table 2 shows the occurrence of X-ray diffraction peaks, from the Figure 3÷7

Table 2.
Data set of diffractometer trace of Figure 3÷7

peak	*hkl*	phase	A	B1	B2	B3	C
1	(112)	cementite		+			
	(021)	cementite		+			
2	(200)	cementite	+	+	+	+	+
3	(210)	cementite		+			
4	(022)	cementite	+	+	+	+	+
	(110)	Fe_α	+	+	+	+	+
5	(211)	cementite	+				
6	(212)	cementite	+				
7	(113)	cementite		+	+	+	+
	(202)	cementite		+	+	+	+
8	(023)	cementite	+	+	+	+	+
	(220)	cementite	+	+	+	+	+
	(004)	cementite	+	+	+	+	+
9	(200)	Fe_α	+	+	+	+	+
	(132)	cementite	+	+	+	+	+

Tables 1 and 2 shows, that the in analyzed areas A, B and C different results of X-ray diffraction were obtained. This applies to the occurrence of the peaks and their intensity values. Peaks 1, 3, 5 and 6 (Tab.2) were observed only in single cases: peaks 1 and 3 in area B1, peaks 5 and 6 in area A. In contrast, only in area A there is no peak 7. In area B, depending on the direction and the way of the test (included sample), different results were obtained.

The calculated values lattice parameter of cementite where listed in Table 3. For cases A, B and C: values in italics are calculated on the basis of indicators *(hkl*), other values were calculated based on the formulas of [11].

5. Summary

The research the results of X-ray diffraction shows, that the impact on do not have the chemical composition or structure phase, that were same for the whole sample.

When tested area B, the arrangement of the sample relative to the goniometer axis was parallel and perpendicular. They also sample included in the resin were tested.

Table 3.
Values of *a, b, c* lattice parameter of cementite

Area	*a*, nm	*b, nm*	*c, nm*
[5]	0.45165	0.50837	0.67475
[7]	0.5076	0.4514	0.6757
[12]	0.48190	0.64774	0.42805
	0.50080	0.67254	0.44650
[13]	0.5092	0.6741	0.4527
[14]	0.45246	0.50884	0.67423
A	*0.45401*		*0.67744*
	0.45480	0.51049	0.67996
B1	*0.45310*		
	0.45369	0.51596	0.67556
B2	0.45356		*0.677*
	0.4534	0.50962	0.68090
B3	*0.45404*		*0.67652*
	0.45434	0.50954	0.68012
C	*0.45401*		*0.67744*
	0.45480	0.52060	0.67793

The *d*-spacings of lattice planes depend on the size of the elementary cell and determine the position of the peaks. For each B

variant other values of the parameters *a, b* and *c* were obtained. This may be the result of directional solidification of ledeburite. In Figure 2b) structure of texture can be seen. The intensity of each peak is caused by the crystallographic structure, the position of the atoms within the elementary cell and their thermal vibration.

The line width and shape of the peaks may be derived from conditions of measuring and properties - like particle size - of the sample material. Rapid solidification may cause a deformation of the lattice plane [6, 7] which is indicated by different values of the lattice parameters (Tab. 3). Such deformation could also be the result of directional solidification

The present study should be continued.

References

[1] Jiyang, Z. (2009). Colour metallography of cast iron. Chapter 5–White cast iron. *China Foundry*, 447-462.

[2] Kagawa, A., Okamoto, T. & Matsumoto, H. (1987). Young's modules and thermal expansion of pure iron-cementite alloy castings. *Acta Materialia.* 35(4), 797-1000.

[3] Mangan, M.A. & Shiflet, G.J. (1999). The Pitsch-Petch orientation relationship in ferrous pearlite at small undercooling. *Metallurgical and Materials Transactions.* 30A, 2767-2781.

[4] Gonser, U., Ron, M., Ruppensberg, H., Kuene, W. & Trautwein, A. (1972). Spin orientation determination by correlating X-ray textures with Mössbauer line intensities in Fe_3C. *Physica Status Solidi (a).* 10(2), 493-499.

[5] www.msm.cam.ac.uk/phase-trans/2003/Lattices2/cementite.data.txt

[6] Hartmann, S. & Ruppersberg, H. (2009). Thermoelastic strain of the lattice plane spacings in white cast iron. *Materials Science and Engineering A.* 325, 153-159.

[7] Battezzati, L., Baricco, M. & Curiotto, S. (2005). Non-stoichiometric cementite by rapid solidification of cast iron. *Acta Materialia.* 53, 1849-1856.

[8] Nikolussi, M., Shang, S.L. & other (2008). Extreme elastic anisotropy of cementite, Fe_3C: first principles calculations and experimental evidence. *Scripta Materialla.* 59, 814-817.

[9] Trepczyńska-Łent, M. (2013). Possibilities of the materials properties improvement for the cementite eutectic by means of unidirectional solidification. *Archives of Metallurgy and Materials.* 58(3), 987-991.

[10] Jenkins, R. (2000). X-ray Techniques: Overview in Encyclopedia of Analytical Chemistry (pp.13269-13288) In R.A. Meyers (Ed.), John Wiley & Sons Ltd: Chichester.

[11] Senczyk, D. (1974). *Laboratory of X-ray crystallography.* Poznań: Ed. Poznan University of Technology.

[12] Lv, Z.Q., Zhang, F.C., Sun, S.H. & other (2008). First-principles study on the mechanical, electronic and magnetic properties of Fe_3C. *Computational Materials Science.* 44, 690-694.

[13] Herbstein, F.H. & Smuts, J. (1964). Comparison of X-ray and neutron-diffraction refinements of the structure of cementite Fe_3C. *Acta Crystallographica.* 17, 1331-1332.

[14] Stuart, H., Ridley, N. (1966). Thermal expansion of cementite and other phases. *Journal of the Iron and Steel Institute*. 711-717.